

Monte Carlo Simulation of Stopped Muon Monitors for DUNE/LBNF

Andrew Loeliger
Department of Physics

Honors Committee:

Advisor: Eric Zimmerman (Physics)

Honors Council Representative: John Cumalat (Physics)

Non-Department Member: Katherine Stange (Math)

April 11, 2016

Abstract

The composition of neutrino flavor eigenstates in terms of neutrino mass states leads to the phenomenon of “neutrino oscillation”, whereby a neutrino created in one flavor may change to another in flight. DUNE (Deep Underground Neutrino Experiment) is an experiment designed with a 1300 *km* baseline to study and measure the parameters involved in neutrino oscillation. To measure the tertiary muon beam created with the neutrinos, a detector designed to measure stopping muons is used. The detector will pick up light created in the decay of a muon in mineral oil in the center. To study the response of the muon monitor in the proposed experiment set-up Monte Carlo simulations using the Geant4 software package is used. Combining a detector specific Monte Carlo simulation with the overall experiment beam Monte Carlo has led to a model for predicting stopping muon flux from an overall muon beam flux. This has been used to create a picture of detector response in arbitrary configurations and develop a timing scheme to prevent saturation of the detector. Progress has also been made using this model to understand detector response using different production models.

Contents

1	Introduction	1
1.1	Physics Background	1
1.2	LBNF/DUNE	3
1.3	Overview of this Thesis	4
2	Neutrino Oscillations and Beams	5
2.1	Neutrino Oscillations	5
2.2	Creation of Neutrino Beams	7
3	The DUNE/LBNF Beamline	9
3.1	The Hadron Absorber and Muon Alcoves	9
3.2	The Near and Far Detectors	13
4	Stopped Muon Monitor Principles	18
4.1	Detector Design and Physics	18
4.2	Geant4 Simulations	21
5	Monte Carlo Simulations of the Stopped Muon Monitor	23
5.1	Measuring Post-Absorber Beam Conditions	23
5.2	Angular and Direct Acceptance of the Stopped Muon Monitor	28
5.3	Inner Detector Signal	35
5.4	Beamline Ramifications	37
5.5	Simulations Under Different Physics	42
6	Future Work and Conclusions	44
6.1	Future Work	44
6.2	Conclusions	45

List of Figures

3.1	The proposed beamline at the near site	11
3.2	Cross section view of the Hadron Absorber	11
3.3	The proposed Absorber Hall	13
3.4	The current Near Detector design	14
3.5	The DUNE Far Detector.	16
4.1	The Stopped Muon Monitor	20
5.1	First tracking plane flux for 10^6 POT	24
5.2	Tracking plane μ^+ flux for 10^6 POT	25
5.3	Tracking μ^- flux for 10^6 POT	25
5.4	Mu θ vs. Energy in the first tracking plane	27
5.5	Low energy mu θ vs. Energy in the first tracking plane	28
5.6	Angular muon hits on a detector for 10^7 POT	30
5.7	Direct muon hits on a detector for 10^7 POT	31
5.8	Spatial profiles of the generated muon set.	32
5.9	Likelihood of a muon at a given energy to stop in the detector	33
5.10	Fits to muon stopping chance data	34
5.11	Other attempted fits to muon stopping chance data	34
5.12	Muon stopping probability for the inner detector	36
5.13	Number of stopping muons seen in a detector after the first shielding block	38
5.14	Stopping muons seen in detectors as a function of shielding and distance from the beamline.	39
5.15	Estimation of timing until the Stopped Muon Monitor sees reasonable muon signal (≈ 50 muons)	41
5.16	Stopping muon signal for FTFP and QGSP physics	43

List of Tables

2.1	Main kaon decay modes	8
5.1	Muon stopping fit parameters	35

Chapter 1

Introduction

1.1 Physics Background

The Standard Model is the cornerstone of modern particle physics. It acts as both register to the fundamental types of particles and rule book for their interaction. It is also known that the Standard Model does not serve as a complete description for all fundamental phenomena. Consequently, searching for breaks from “Standard Model Physics” motivates current particle physics experiments. One avenue of study in beyond Standard Model Physics comes from neutrinos, a near massless trio of leptons. Neutrinos are denoted by their “flavor” (which correlates them to the more massive leptons: the electron, muon and tau particles). Neutrinos undergo a process called oscillation, which means that in flight, the observed flavor of a neutrino may change, depending on the distance that neutrino has traveled, and its energy.

Neutrino oscillation itself offers multiple avenues of insight into possible new physics. Neutrino oscillation can be described in terms of mixing angles. Neutrino oscillations demonstrate that neutrinos themselves have mass, and the difference of the mixing angles can be used to show that there exist distinct mass states for neutrinos. Furthermore, studying oscillations allows one to determine the differences in the squared masses of the neutrino states. Current oscillation studies tell us about the relation of the first two mass states to each other, but the relation to the third is not yet understood, and the third state may be heavier, or lighter than the the other two states. Detailed study of the pattern of neutrino oscillation will allow for the determination of the neutrino mass state ordering. The neutrino mass states themselves are also related to another important question in neutrino physics, that is the question of whether neutrinos are their own anti-particles (“Majorana” particles).

Another area of investigation in neutrino physics is the possible presence of charge parity (CP) symmetry violations. These asymmetries involve a phase difference (δ_{CP}) that changes sign under charge conjugations and parity, and would imply a difference in how both anti-neutrinos and neutrinos oscillate. This has the potential to explain some of the deeper asymmetries of the observed universe, notably, the the vast difference in the amount of observed anti-matter and matter.

1.2 LBNF/DUNE

Neutrino oscillation probability is dependent on both the distance the neutrino has traveled and the energy of the neutrino. This means experiments must be carried out over long distances in order to have detectors in peak oscillation regions. The Deep Underground Neutrino Experiment (DUNE, Formerly LBNE¹) and its hosting facility LBNF (Long Baseline Neutrino Facility) will be a next generation accelerator experiment aimed at studying these out standing questions in neutrino physics through precise observation of neutrino oscillation.

DUNE will utilize a 1300 km baseline originating at LBNF at the Fermi National Accelerator Laboratory (FNAL or Fermilab), and terminating at the Sanford Underground Research Facility (SURF) at the Homestake Mine at Lead, SD. DUNE is aimed at precision measurements of neutrino oscillation parameters (particularly θ_{23} , θ_{13} and δ_{CP}) as a means for establishing the neutrino mass hierarchy and establishing the extent of CP violations in neutrino mixing. To accomplish this, two detectors are deployed along the beamline at the near and far sites to measure the extent of neutrino oscillations over the length of the experiment. To maintain the precision demanded by these measurements, DUNE will not only be using its two main detectors, but also a suite of secondary beamline monitors measuring muons in order to maintain control of beam direction and knowledge of overall beam com-

¹Long Baseline Neutrino Experiment

position. There are three types of muon monitoring systems slated for use at LBNF: Gas Cherenkov Monitors, Diamond Detectors, and Stopped Muon Monitors.

1.3 Overview of this Thesis

This thesis will provide an overview of the methods currently used to predict the performance of the Stopped Muon Monitor in the DUNE beamline. Chapter 2 of this thesis will focus on the neutrino beam itself, detailing both oscillation and the production of the beam. Chapter 3 will focus on the near site facilities available to LBNF/DUNE and the proposed deployments of the muon monitoring systems. Chapter 4 will focus on the operation of the Stopped Muon Monitor system. Chapter 5 will detail the current methods for studying the Stopped Muon Monitor, and what that implies for the operation of the Stopped Muon Monitor and DUNE. Chapter 6 will discuss conclusions and the future of the Stopped Muon Monitor.

Chapter 2

Neutrino Oscillations and Beams

2.1 Neutrino Oscillations

Neutrino oscillation can be understood as the relationship between the two most useful bases for describing neutrinos, the mass and flavor eigenstates. The basis vectors in the two bases are mixed in terms of the other basis vectors, and it is from this that neutrino oscillations arise. To elaborate, we can draw from a derivation performed by C. Giunti [1], if we have a neutrino in a state $|\nu_a\rangle$, where $a = e, \mu, \tau$ is one of the flavor eigenstates, then these states are related to the mass eigenstates (call them $|\nu_b\rangle$ where $b = 1, 2, 3$) by

$$|\nu_a\rangle = \sum_{b=1}^3 U_{ab}^* |\nu_b\rangle, \quad (2.1)$$

with U a unitary matrix called the Pontecorvo-Maki-Nakagawa-Sakata (PMNS) matrix. The PMNS matrix is dependent on three mixing angles that define how the states are composed[2, 3]. The PMNS matrix is more commonly expressed in a decomposed form

$$U = \begin{pmatrix} 1 & 0 & 0 \\ 0 & c_{23} & s_{23} \\ 0 & -s_{23} & c_{23} \end{pmatrix} \begin{pmatrix} c_{13} & 0 & e^{i\delta_{CP}} s_{13} \\ 0 & 1 & 0 \\ e^{i\delta_{CP}} s_{13} & 0 & c_{13} \end{pmatrix} \begin{pmatrix} c_{12} & s_{12} & 0 \\ -s_{12} & c_{12} & 0 \\ 0 & 0 & 1 \end{pmatrix}, \quad (2.2)$$

where $s_{xy} = \sin \theta_{xy}$ and $c_{xy} = \cos \theta_{xy}$. To show the effect this has on neutrino flavor states one can apply the Schrödinger equation to find:

$$i \frac{\partial}{\partial t} |\nu_b\rangle = \hat{\mathbf{H}} |\nu_b(t)\rangle = E_b |\nu_b\rangle. \quad (2.3)$$

Which means under time evolution one finds that:

$$|\nu_b(t)\rangle = e^{iE_b t} |\nu_b(t=0)\rangle. \quad (2.4)$$

From here one can rewrite flavor states in terms of mass states and find that:

$$|\nu_a(t)\rangle = \sum_b U_{ab}^* e^{-iE_b t} |\nu_b(t)\rangle = \sum_{c=e,\mu,\tau} \left(\sum_b U_{ab}^* e^{-iE_b t} U_{cb} \right) |\nu_c\rangle \quad (2.5)$$

Thus, a neutrino created in a flavor state ‘a’ will evolve in time to be a superposition of other flavor states as dictated by the PMNS matrix.

2.2 Creation of Neutrino Beams

To produce a dedicated source of neutrinos to study the oscillation parameters poses an interesting problem. Neutrinos are electrically neutral, and they do not feel the strong force, which means that all neutrino decays and interactions are governed by the weak force. This means that to create a dedicated neutrino beam, one must have a weakly decaying parent particle that can be easily manipulated and focused. A typical choice of parent particle is charged pions. Charged pions decay via the process(es):

$$\pi^\pm \rightarrow \mu^\pm + \nu_\mu^{(-)} \quad (2.6)$$

more than 99.9% of the time[4]. Charged pions can be created in the interaction of high energy protons on carbon, and the DUNE target is composed of carbon to take advantage of this process [5, 6]. Also to be noted in the pion decay process, is the creation of muons in the decay. This creates a secondary beam of muons alongside the primary neutrino beam. Many of

Main Kaon Decay Modes	
$K^+ \rightarrow \mu^+ \nu_\mu$	63.55%
$K^+ \rightarrow \pi^+ \pi^0$	20.66%
$K^+ \rightarrow \pi^+ \pi^+ \pi^-$	5.59%
$K^+ \rightarrow \pi^0 e^+ \nu_e$	5.07%
$K^+ \rightarrow \pi^0 \mu^+ \nu_\mu$	3.353%
$K^+ \rightarrow \pi^+ \pi^0 \pi^0$	1.761%
$K_S^0 \rightarrow \pi^+ \pi^-$	69.20%
$K_S^0 \rightarrow \pi^0 \pi^0$	30.69%
$K_L^0 \rightarrow \pi^\pm e^\mp \nu_e$	40.55%
$K_L^0 \rightarrow \pi^\pm \mu^\mp \nu_\mu$	27.04%
$K_L^0 \rightarrow \pi^0 \pi^0 \pi^0$	19.52%
$K_L^0 \rightarrow \pi^+ \pi^- \pi^0$	12.54%

Table 2.1: Main kaon decay modes. All modes with $> 1\%$ probability of occurring. K^- modes are charge conjugates of K^+ modes. Data taken from [4]

the statistics of this muon beam (such as beam center and energy spectra) are related to the neutrino beam. This forms the basis of muon monitoring as a method for studying neutrino beams.

Proton collisions on carbon can also create kaons. Kaons form a significant portion of the post target beamline, and as such, their contributions must be considered[3]. Fortunately charged kaons decay most frequently into several convenient modes, seen in Table 2.1.

Chapter 3

The DUNE/LBNF Beamline

3.1 The Hadron Absorber and Muon Alcoves

Immediately after the proton interactions in the LBNF target, the beam is now composed of secondary charged mesons, secondary protons and neutrons, and primary protons that did not interact in the target. To achieve the focusing required to project the neutrinos into a beam, the charged mesons are magnetically focused[6]. The large momentum carried by these parent mesons in the lab frame ensure that in the eventual decay to neutrinos, the daughter particles from the decay will maintain the profile of the mother particles.

To facilitate this process, immediately after the target hall enclosure are two magnetic “horns”[6] (referred to as such because of their unique shape) that are responsible for creating a toroidal magnetic field. Through a simple

application of the Lorentz Force Law it can be seen that in such a toroidal magnetic field, particles of a chosen charge sign can be focused inwards towards a central point. Equally as important, particles of the opposite charge sign will be deflected outwards. This sign selection potential is the mechanism behind creating beams of specifically neutrinos or anti-neutrinos.

After the magnetic horn volumes, the beamline goes through a 200 m long cylindrical decay volume, known as the decay pipe. In this volume, the secondary charged beam particles are given the opportunity to decay into the neutrino beam and all tertiary particles [5, 6].

Immediately after the decay pipe volume are the Hadron Absorber and the Muon Alcoves. The Hadron Absorber is a large box of concrete with a core of aluminum and steel modules. The Hadron Absorber serves as a beam dump for uninteracted primary protons which may have escaped the target, or for secondary hadrons that failed to decay in the decay region[5, 6]. The Absorber itself is composed of a core assembly, made of aluminum and steel slab segments, surrounded by concrete. After the hadron absorber, the only significant contribution to the beam will be the muon beam and the throughgoing neutrino flux.

After the Hadron Absorber are the Absorber Hall and Muon Alcoves [3, 5]. The area behind the hadron absorber provides the best opportunity for making muon measurements with minimal background. To take advantage of this, inside this hall the three types of muon monitoring systems will be deployed. The first two systems consist of diamond ionization counters,

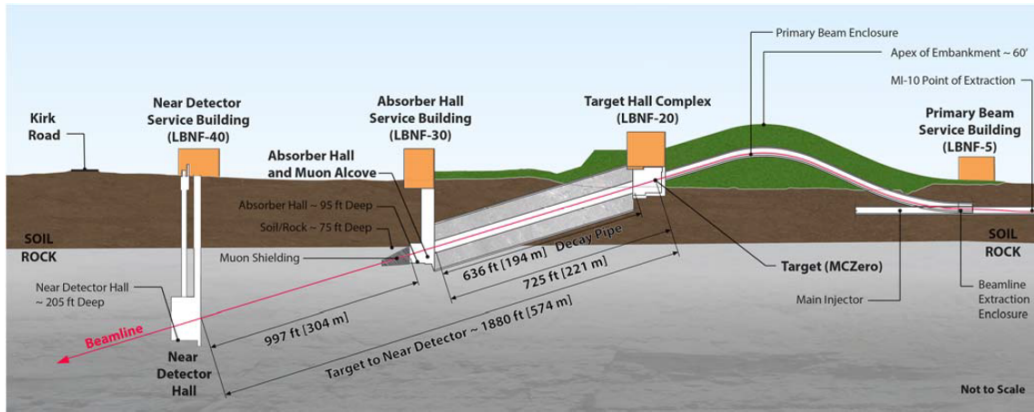


Figure 3.1: The proposed beamline at the near site. Figure taken from [6])

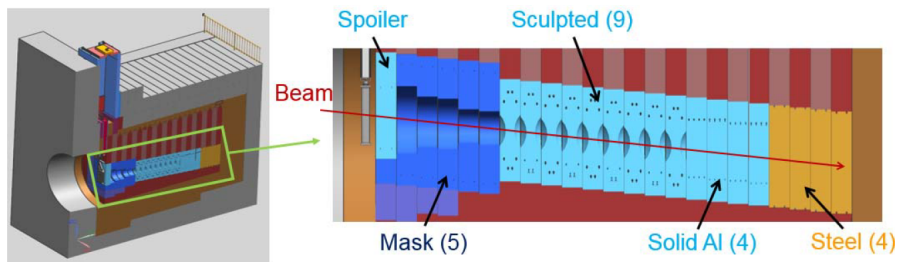


Figure 3.2: Cross section view of the Hadron Absorber. Figure taken from [6]

which uses muon energy deposited in the diamond to register an electrical signal, and the Gas Cherenkov Muon Monitor, which uses Cherenkov radiation to measure through going muons[7]. These systems are deployed almost immediately after the alcove end of the absorber. The final system, and the focus of the rest of this thesis, is the Stopped Muon Monitor. The Stopped Muon Monitor is arranged at multiple points along the 10 m length of the muon alcoves.

The Stopped Muon Monitors will be interspersed between layers of steel shielding called “blue blocks”. The steel shielding serves to stratify muons by energy, and the Stopped Muon Monitors pick up muons that stop immediately after the shielding block[7]. Muons that have enough energy so that they don’t stop may stop after going through another shielding layer, and this allows for energy spectra measurements from the stopped muon monitors. The energy spectra of the muons can then serve as a predictive tool for the energy spectra of the neutrino beam itself[7]. Furthermore, for each layer of shielding, the Stopped Muon Monitors are arrayed in crosses, and by careful observation of strength of muon signals in specific monitors in a cross, and between layers of shielding, precision measurements of the center of the muon beam can be made. Given the large forward boost the muon and neutrino beam have at creation, the two beam centers are highly correlated, and the neutrino beam center can be predicted with this measurement of the muon beam center.

To meet the needs of the DUNE beamline, the muon monitors will be able

to measure the incoming muon flux to within 5%. This will allow for similar accuracy measurements for muons above 6 GeV[7]. Beamline stability is also essential, and to keep energy stable to within 1% across all energy bins, the neutrino beam must be constrained to within 0.2 mrad. This corresponds to being able to place the post-absorber muon beam center to within 5 cm[7].

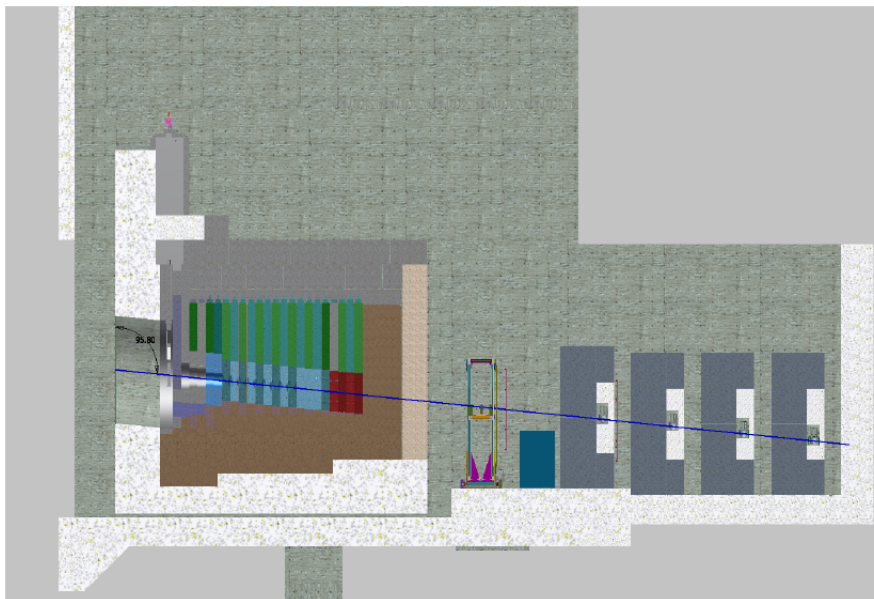


Figure 3.3: The proposed Absorber Hall. The Hadron Absorber is on the left hand side of this photo and the various stopped muon monitors are aligned with the steel shielding blocks going to the right. Figure taken from [7]

3.2 The Near and Far Detectors

Approximately 300 m after the end of the Absorber Hall lies the DUNE Near Detector. The Near Detector makes the initial measurements of the neutrino beam which provides the appropriate initial conditions to the appearance

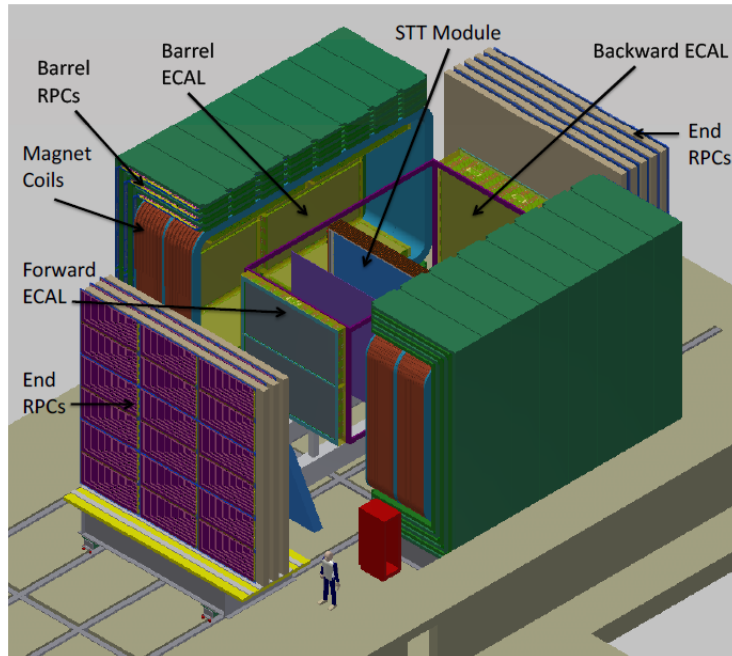


Figure 3.4: The current Near Detector design. The detector is pulled apart to demonstrate the technologies involved and a person is included for reference. Figure taken from [7]

and disappearance measurements made at the Far Detector [2]. The Near Detector is a Fine Grain Tracking system composed of a central Straw Tube Tracker, Electromagnetic Calorimeter, and Muon Identifier Systems.

The Straw Tube Tracker forms the central portion of the near detector, and is highly modular[7]. It is composed of small (1 cm outer diameter) “Straw Tubes” filled with pressurized argon or xenon gas. Neutrino interactions in these materials will produce charged leptons, that can be picked up as an electrical signal on gold wiring in the tube. Argon is used in the DUNE far detector as a detection material, and the argon modules are expected

to be able to provide almost ten times the amount of unoscillated neutrino statistics than the far detector would provide[7]. The xenon equipped modules will be followed by specifically designed radiators and both the xenon and the radiators will be used to distinguish positrons and electrons in the the Straw Tube Tracker [7]. Positron/electron identification forms the basis of neutrino/antineutrino identification.

The Straw Tube Tracker itself is surrounded on all sides by electromagnetic calorimeters (ECALs)[7]. The electromagnetic calorimeter uses layers of alternating scintillator bars separated by lead sheets and wavelength shifting fibers. Light from the fibers is read into a silicon photomultiplier photosensor and this forms the basis of the ECAL signal.

The other components of the Near Detector assist include the surrounding dipole magnet, and the Muon Identification chambers[7]. The dipole magnet will put a 0.4 T field through the ECAL and Straw Tube Tracker segments, which will allow for the measurement of particle momentum and charge as it passes through these detector volumes[7]. The Muon Identification chambers will identify muon tracks and differentiate them from charged hadron tracks via the ability of a muon to penetrate iron without creating showers.

The DUNE Far Detector design is somewhat in flux, but the core design involves the usage of a multi-kiloton liquid argon time projection chamber (TPC)[7]. The DUNE Far Detector is designed to be installed in 10kt modules of liquid argon [5]. To maintain the liquid argon and high precision electronics necessary for precision measurement and low noise current mea-

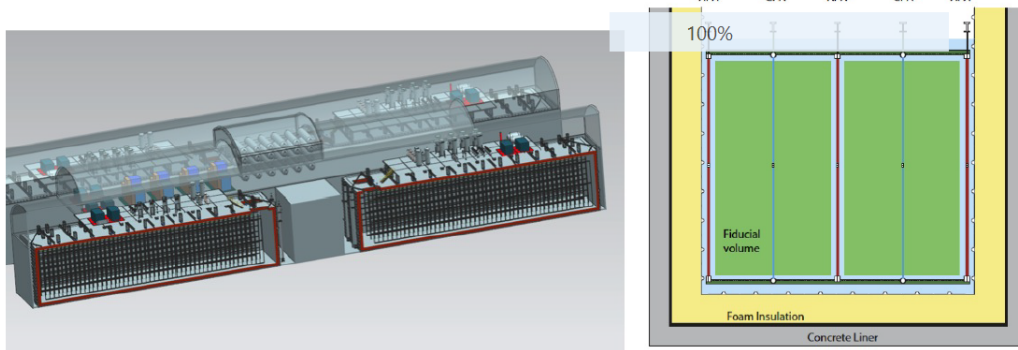


Figure 3.5: The DUNE Far Detector. The left figure shows a rendering of what the completed detector will be, with visible wire detection planes. The right image shows a cross section of the fiducial volume with anode and cathode planes marked. Figure taken from [7]

measurements, the 10kt modules are constructed in cryostats. Using these precision electronics, the DUNE Far Detector will reach a 9:1 signal to noise ratio [7]. The interaction of neutrinos in the liquid argon will produce electron/ion pairs and scintillation light. The TPC is interspersed with high-voltage anode and cathode wire planes to detect charged particles. The use of multiple wire planes in different transverse directions allow for measuring charged tracks in 3 dimensions.

To identify neutrino species detected in the far detector, identification of muon and electron tracks in the TPC is necessary. Stopping muons in the TPC can be identified by observing and reconstructing the decay, and uncontained muons can be observed by observing the angle from the beam. Implicit in these measurements of charge observed in the TPC is the measurement of momentum and energy of the observed leptons. These measurements allow

the measurement of the muon and electron neutrino energy spectra, which is a parameter of neutrino oscillation fits.

Chapter 4

Stopped Muon Monitor

Principles

4.1 Detector Design and Physics

As mentioned previously, stopped muon monitoring offers a variety of benefits to the DUNE beamline. Accurate measurement of the muon flux will provide a means by which to constrain the expected flux at both the near and far detectors. The muon monitors also provide a means to measure and maintain the neutrino beam center.

The Stopped Muon Monitor itself utilizes two primary detector volumes to detect muon events. The inner volume is a mineral oil center filled with a former Exxon product known as Marcol 7 that was used at the MiniBooNE experiment[8]. This volume forms the bullet shaped center of the detector,

and serves to pick up the Cherenkov light emitted in muon decay. Muons decay by the process(es):

$$\mu^- \rightarrow e^- + \bar{\nu}_e + \nu_\mu, \quad (4.1)$$

$$\mu^+ \rightarrow e^+ + \nu_e + \bar{\nu}_\mu. \quad (4.2)$$

Muons have a mass of $\approx 105 \text{ MeV}/c^2$. This is about 200 times greater than the electron (or positron) mass, and greater than any of the neutrino mass states. This means that the charged lepton produced in muon decay will have a significant momentum coming out of the decay.

Charged particles that would otherwise be going faster than the speed of light in a medium radiate. This process is called Cherenkov radiation[9]. This radiation can be picked up as an electrical signal with the use of photomultiplier tubes (PMTs). Since decay electrons produced in a stopped muon decay are isotropic, the Cherenkov cone can be as well. To ensure that the most amount of signal is extracted from the Cherenkov material, four PMTs are deployed in a ring around the top of the inner detector volume. The Cherenkov material that fills the inner detector also scintillates under incident charge, but this does not form the core signal that the Stopped Muon Monitor was developed to measure.

To try to veto extraneous signals, another shell volume is placed around the inner detector volume. This volume is called the Liquid Scintillating Veto, or Outer Detector. This volume is filled with a liquid scintillator that will scintillate heavily under incident charge. To pick up this scintillation light,

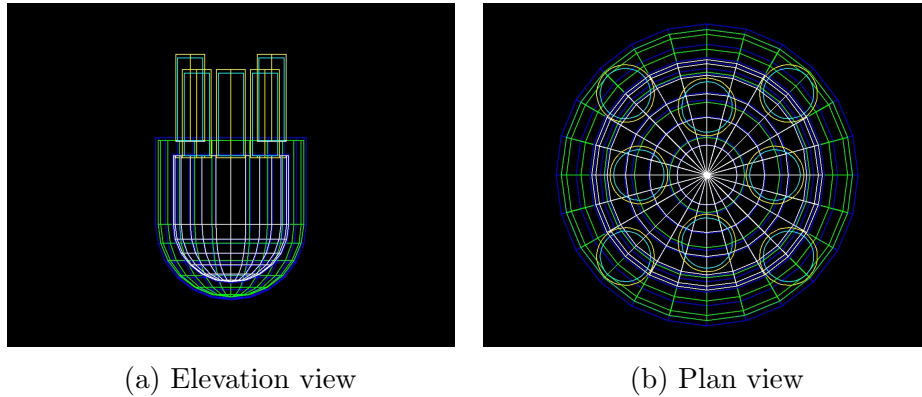


Figure 4.1: The Stopped Muon Monitor. The green volume is the liquid scintillating veto, and the white volume is the mineral oil. The eight pmt tubes are shown as the cylinders coming out of the detector. The tubes closest to the center look into the inner detector, whereas the tubes further out look at the liquid scintillating veto.

four more PMTs are used to detect this veto signal. Since the muon lifetime itself is far greater than the time needed for beam particles to traverse the detector, simultaneous detector signals can be vetoed as not stopped muon events and partially contained events can be excluded as well. Furthermore, to prevent saturation of detector PMTs, the inner detector PMTs are gated. As part of operation, PMTs are kept at high voltages to detect tiny signals. Excess light in the PMT face can cause damage to the tube, so gates on the pmt are used to block light until the tube is ready for operation. In normal beam operation the gates can be triggered based on the timing of the beam pulses.

This gives typical beam operation in the detector a very defined structure. The initial beam pulse coincides with starting a timer on the PMT gates in

the Stopped Muon Monitor. In the course of a beam pulse, the overall stopping muon flux in the detector can be millions of muons, but many decay before the PMT gates are triggered. After the gates are triggered, signal collection in both detector volumes can begin. Typical events in the detector will have muons decay and Cherenkov radiation will be picked up on the inner detector PMTs. Any events where the decay electron escapes the detector or a particle traverses the detector will create scintillation light in the veto which is picked up on the veto PMTs. These events are subject to veto. The pulses of light seen in the inner detector can be measured and absolute through-going flux can be inferred.

4.2 Geant4 Simulations

To study detector performance without the need for complicated or expensive beamline elements, computer modeling and simulation is used. Two specific Monte Carlo simulations are used in the development of the Stopped Muon Monitor. The first is the in-detail stand-alone detector simulation of the Stopped Muon Monitor, used for doing detailed work on the nature and amount of response under specific conditions. The second is the more general DUNE/LBNF beamline Monte Carlo (G4LBNE, now updated to G4LBNF), detailing the full beamline more generally, starting at the carbon targets and tracking through the end of the muon alcoves. The chosen Monte Carlo software package that drives both simulations is called Geant4.

Geant4 is a dedicated framework for the simulation of particle interaction developed by CERN[10]. Geant4 is highly customizable, and can be programmed with specific materials and physics processes to suit the problem at hand. As long as the basic properties of a material are known (things such as density, atomic composition and scintillation properties) these materials can be added to the overall beam and detector geometry. The initial particles of any simulation can be customized to give arbitrary geometric and angular distributions, which allows testing multiple complex beam setups with relative ease. In terms of practical applications to the Stopped Muon Monitor, this also means that specific detector volumes can be singled out and tested individually, or an incident beam from the rest of the DUNE experiment can be simulated. Geant also runs on an event-by-event basis, allowing for information taken from the simulation to be handled piecemeal. Individual properties about particles are stored in the particle's track. This information is comprised largely of kinematic and position information, but can include some information about the parent particle and process which created the current particle. The data extracted from both simulations is handled using another object-oriented CERN-developed software framework called ROOT [11].

Chapter 5

Monte Carlo Simulations of the Stopped Muon Monitor

5.1 Measuring Post-Absorber Beam Conditions

To understand muon monitor performance, beam conditions immediately after the end of the absorber need to be understood and accurately modeled. The beam Monte Carlo itself lacked any simulation of the steel shielding layers, which are vital to understanding the performance of the Stopped Muon Monitor. Standard steel shielding “blue blocks” are 3 ft in width. To simulate their post absorber presence, steel planes, 3 ft in depth and 5 m height and width were added starting 4m after the end of the absorber (to approximate where the other muon detectors are), and each plane is 2.7 m

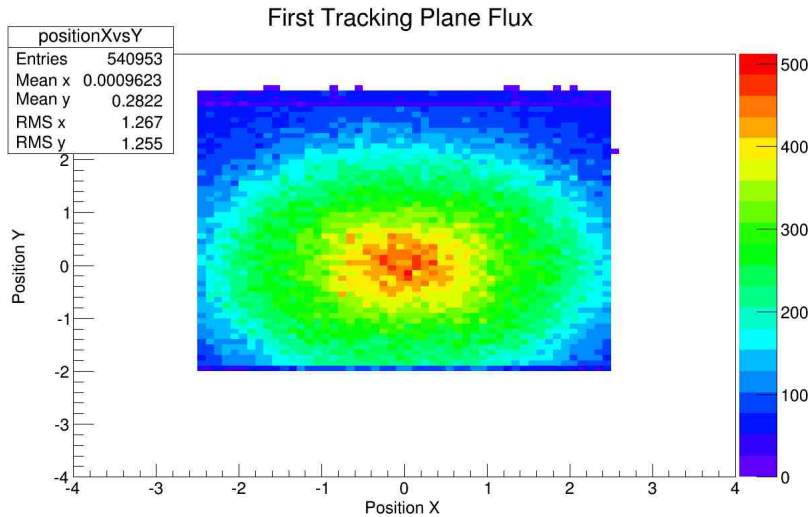


Figure 5.1: First tracking plane flux for 10^6 POT. This serves as a good benchmark for the size and distribution of the post-absorber beam, and confirmation that the simulation is providing sensible results. The overall flux here is not normalized to a standard beam pulse.

apart. This allows for 3 simulated alcoves along the length of the simulated hall.

Immediately behind each of these planes a thin tracking plane was added. The tracking planes are the same simulated air material the rest of the hall that it resides in, but all through-going particles register their passage through the tracking planes. While in the tracking planes, particles have track information recorded. This information includes particle species, position in the tracking plane, vertex (birth) position, and the relevant kinematic information. Another tracking plane was also added immediately preceding the first simulated blue block layer, to understand the the flux immediately post-absorber.

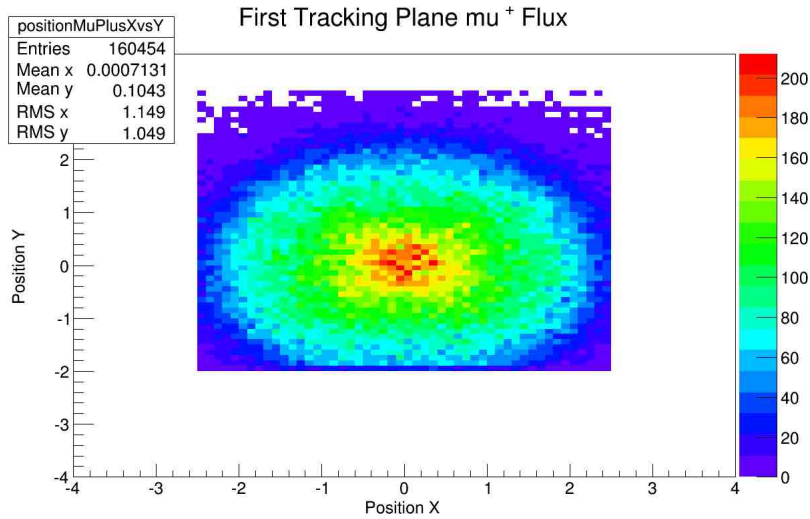


Figure 5.2: Tracking plane μ^+ flux for 10^6 POT. This distribution of muons and beam center is virtually identical to the overall through-going beam flux. This plot assumes running in neutrino mode on the magnetic horns

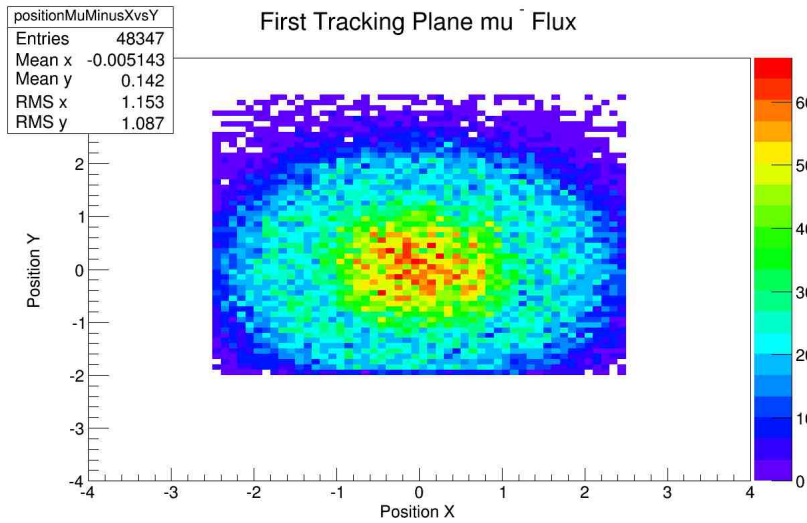


Figure 5.3: Tracking plane μ^- flux for 10^6 POT. This plot assumes that the magnetic horns are focusing positive particles. This distribution has far less overall flux and is much less focused than the corresponding μ^+ distribution, which is exactly as it should be in neutrino mode.

The first simulations run were done with 10^6 protons on target (POT). This is several orders of magnitude lower than what an actual beam pulse at LBNF would encompass, but it serves to demonstrate that the simulation was working and providing sensible results. Overall tracking plane fluxes and specific muon fluxes were assembled for comparison, as seen in Fig(s). 5.1, 5.2, and 5.3.

While these flux plots show a snapshot of overall particle and muon flux before the shielding, they do not provide an adequate description of how the flux is traveling. To study this, angular distributions of muons were reconstructed from their momentum vectors. Plotted against energy this can provide an idea of how all the muon distribution itself moves through the hall. The number of POT was scaled up and the simulations were rerun with 10^7 POT. The results can be seen in Fig. 5.4. Since the Stopped Muon Monitor's signal is comprised of stopping muons, the signal that is seen by the monitor itself would arrive at the post absorber with relatively low energy, and Fig. 10 shows this distribution of muon to arrive with a relatively large angular distribution. To understand the angular distribution of the low energy muons that would be expected to make up the core of Stopped Muon Signal one can look at the low energy section of the muons and rebin. The results of this are in Fig. 5.5.

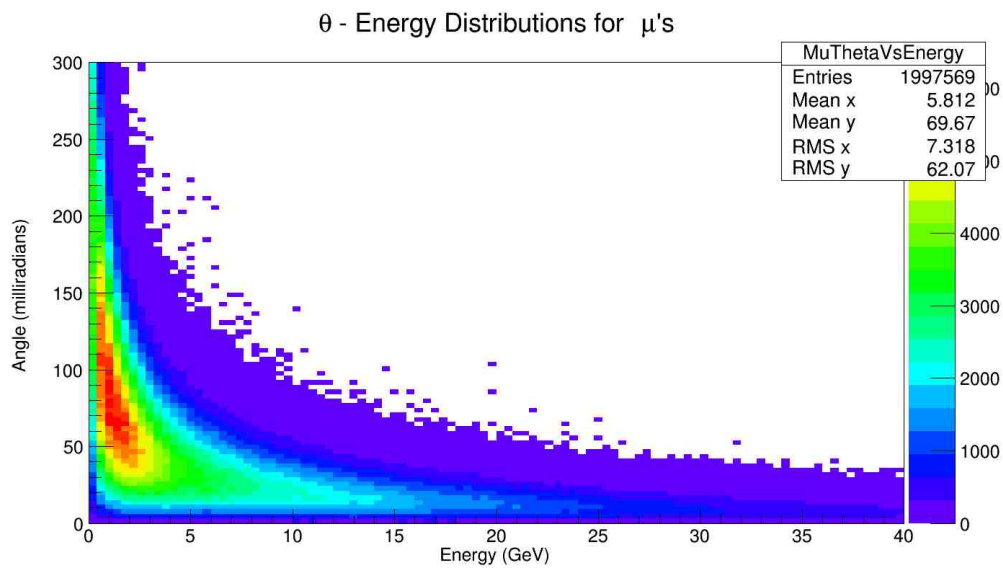


Figure 5.4: Mu θ vs. Energy in the first tracking plane. This is not normalized to a standard beam pulse, but still demonstrates how the muon spectra looks prior to shielding. The angle here is defined to be the angle off the beamline.

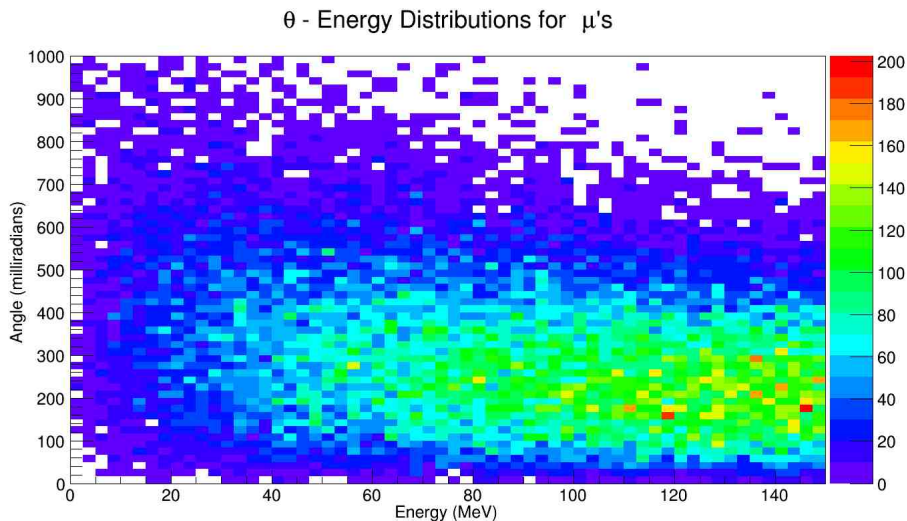


Figure 5.5: Low energy mu θ vs. Energy in the first tracking plane. This is representative of 10^7 POT and not a beam pulse, but still provides a good idea of what the Stopped Muon Monitors would expect to see. The angle here is defined to be the angle off the beamline.

5.2 Angular and Direct Acceptance of the Stopped Muon Monitor

In light of these angular distributions, it is vital to understand the angular acceptances of stopped muon monitors in different positions. To study this, the 10^7 POT data set was used again. At the second tracking plane (the first one behind steel shielding) a random point in the tracking plane was chosen as a “detector center” and a detector face was assumed to be pressed directly up against the tracking plane. From here, the Stopped Muon Monitor was simulated as a rectangular prism and anything that entered through the face of the detector that was pressed up against the tracking plane was excluded.

The muon data was then reanalyzed looking for any muon that would have crossed the tracking plane at a spot not directly inside of the near face, but whose momentum would have caused it to enter the detector. These muons form the angular muons seen in the alcoves. Sample results can be seen in Fig. 5.6. To compare, the same simulation of detector faces was run on the same data set but this time all angular muons were rejected, and direct hits were recorded. Sample results are seen in Fig. 5.7. The number of muons that hit directly on the detector are far far greater than those that would enter from an extreme angle. This analysis with the randomly chosen detector center was done 10,000 times, with similar results for all placed detector centers. Simply estimating from Figs. 5.6 and 5.7, angular muons seem to be $\approx 0.2\%$ of all muons seen entering into the detector.

Direct passage of muons through the detector can be tested in detail using the Stopped Muon Monitor Monte Carlo. A set of 10^8 muons were generated uniformly over the profile of the detector (see Fig. 5.8), and given a uniformly randomized low energy (between 0 and 0.2 GeV) with a momentum directly through the detector (such that it would be tangent at the edge of the profile and directly orthogonal at the center). All generated muons had their initial parameters such as initial position and energy spectrum recorded. Two sets of data were taken, one recording all muons' parameters directly at generation and another for all the through-going muons. The difference of the two data sets was taken to find the set that described muons that stopped in the detector. Ratios were taken from the overall stopping energy spectrum to

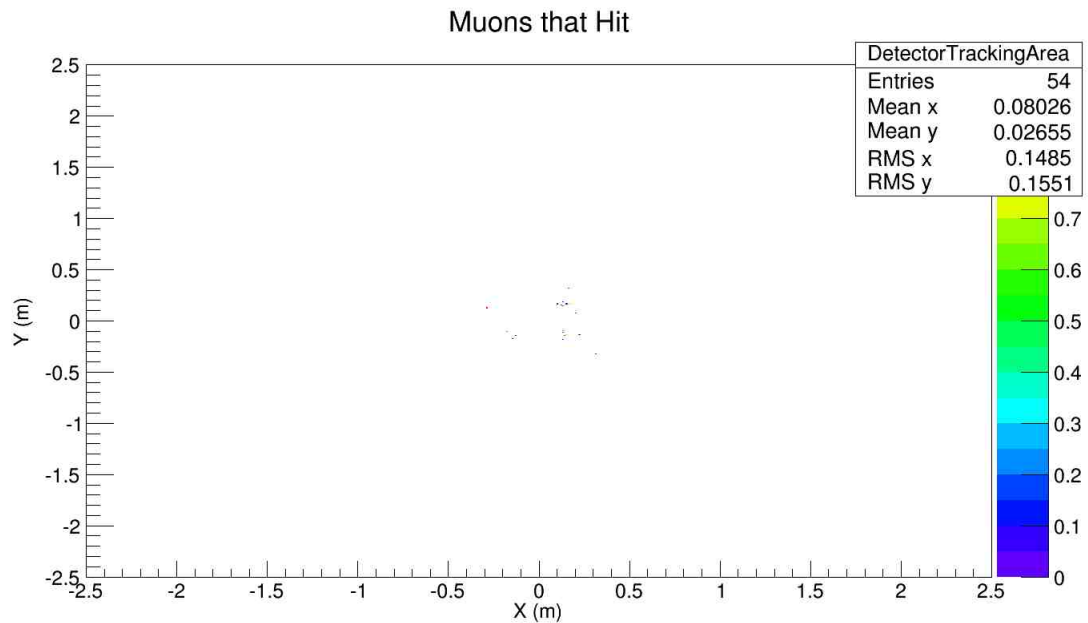


Figure 5.6: Angular muon hits on a detector for 10^7 POT. The simulated detector face in this figure is located just to the right of 0m in the x direction, and just above 0m in the Y direction. The vertical scale here includes importance weighting for the muons, a probability measure that corrects for biased generation. The number of muons seen compared to the number of POT is extremely low, which means that muons entering at extreme angles is a minor effect in the muon alcoves.

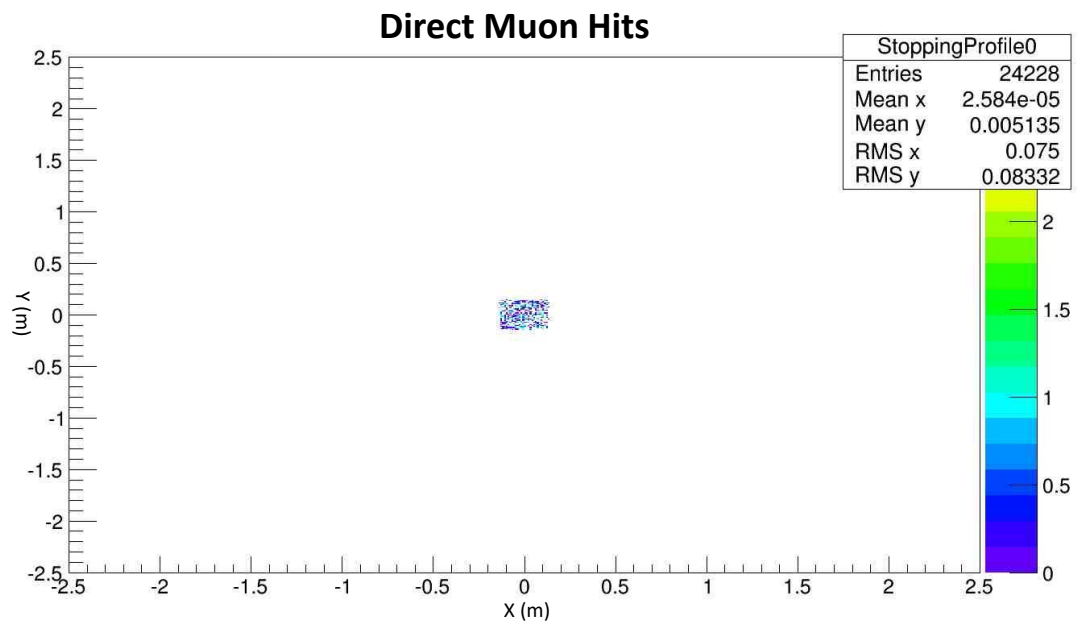


Figure 5.7: Direct muon hits on a detector for 10^7 POT. Note that in comparison to Fig. 5.6, there are significantly more data points. The detector is also placed similarly, slightly to the right of 0m in X and slightly above 0m in Y. The vertical scale here includes importance weighting for the muons, a probability measure that corrects for biased generation.

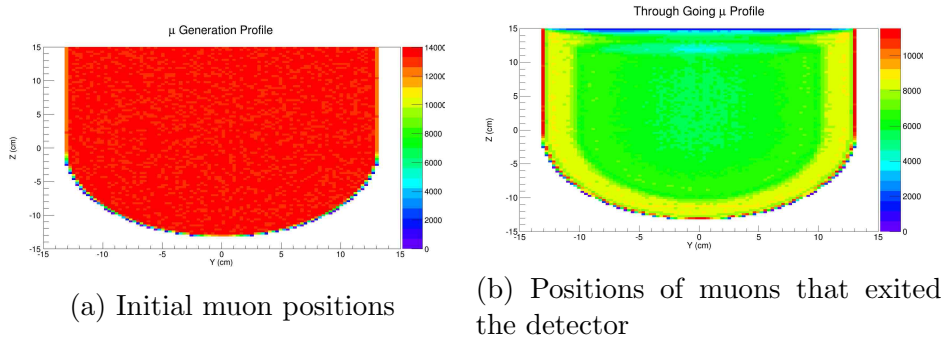


Figure 5.8: Spatial profiles of the generated muon set.

the overall generated energy spectrum. The result, (seen in Fig. 5.9) is a set of data points that describes how likely a given beam muon would be to stop in the detector. This data set is fortunately sigmoidal, which means that empirical fits to the data can be performed with relative ease. Several sigmoid functions with multiple varying parameters each were run through ROOT's function fitter. The results of this can be seen in Figs. 5.10 and 5.11.

The best functional form fit to the data comes in the form of the Gompertz curve, the blue line in Figs. 5.10 and 5.11. The Gompertz curve is a standard actuarial science function that describes mortality laws [12]. More generally, a population or individual that follows the Gompertz curve evolves under time as:

$$y = a^{b^{c \cdot x}}, \quad (5.1)$$

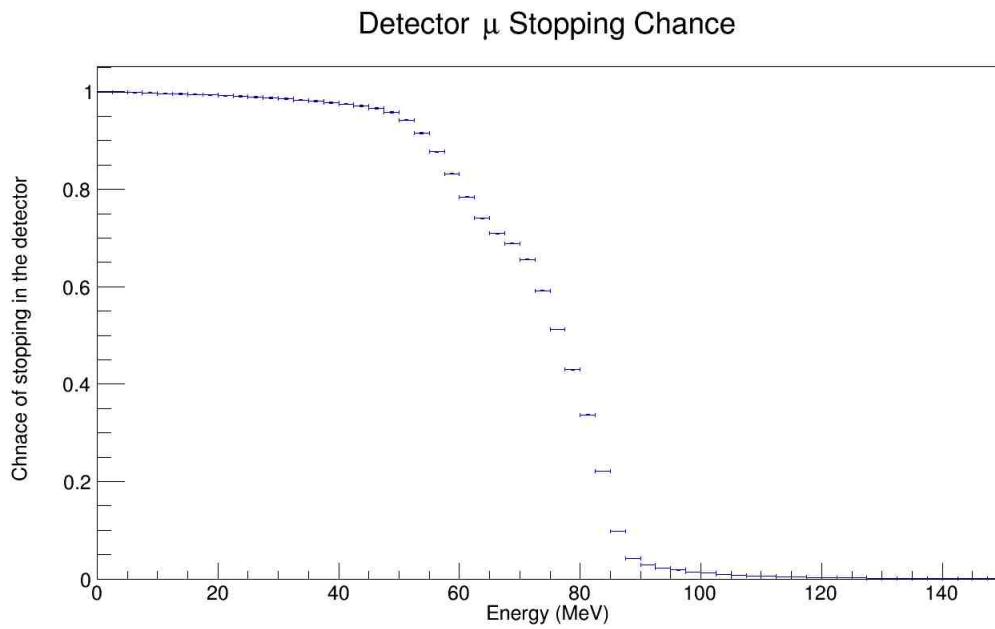


Figure 5.9: Likelihood of a muon at a given energy to stop in the detector. The data goes asymptotically to zero at higher energies, exactly as one would expect. Furthermore the data seems to take a fairly convenient functional form.

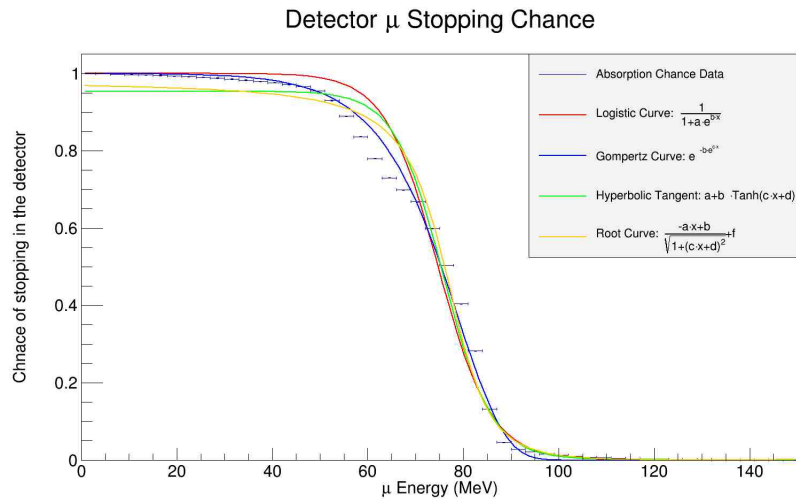


Figure 5.10: Fits to muon stopping chance data. Several functional forms were tried but the best fit that was found was the Gompertz curve (the line in blue). The Gompertz curve is used in actuarial science as a mortality prediction tool.

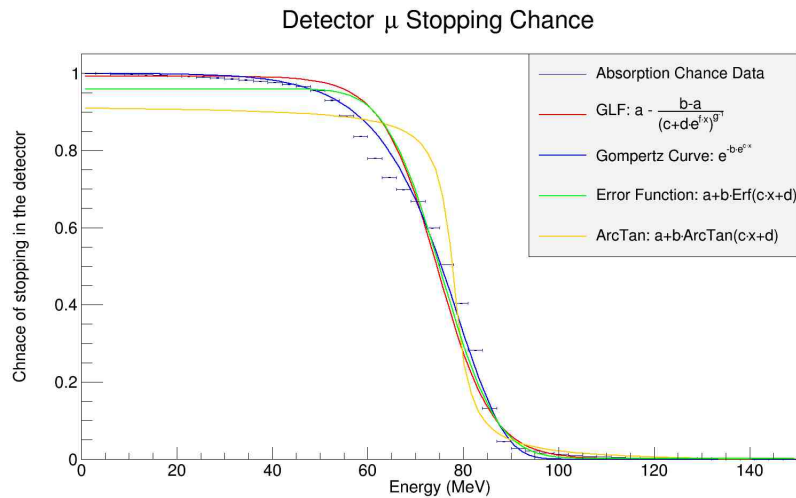


Figure 5.11: Other attempted fits to muon stopping chance data.

Parameter	Value
b	$-3.01077 \cdot 10^{-4}$
c	.102607

Table 5.1: Muon stopping fit parameters.

or equivalently:

$$y = e^{b \cdot e^{c \cdot x}}, \quad (5.2)$$

where x is in MeV.

For our specific use we use the second form of the curve with parameters given in Table 5.1. Knowing the best fit function for muons that stop in the detector allows us to use it as a weighting function for any muons seen in the beamline Monte Carlo. This means that instead of using tracking planes to simply watch what goes through and at what energy, actual numbers of stopping muons can be predicted from overall flux.

5.3 Inner Detector Signal

Briefly, as an aside, it should be mentioned that tests were also performed with the stand-alone detector Monte Carlo to determine the energies of the muons that were seen stopping in the inner detector only. The tests were carried out similar to how the overall stopping chance in the detector was determined. A set of 10^8 muons were simulated with the same overall kinematics, with all muons' initial parameters recorded and then all muons that stopped in the inner detector volume being recorded. From there a similar

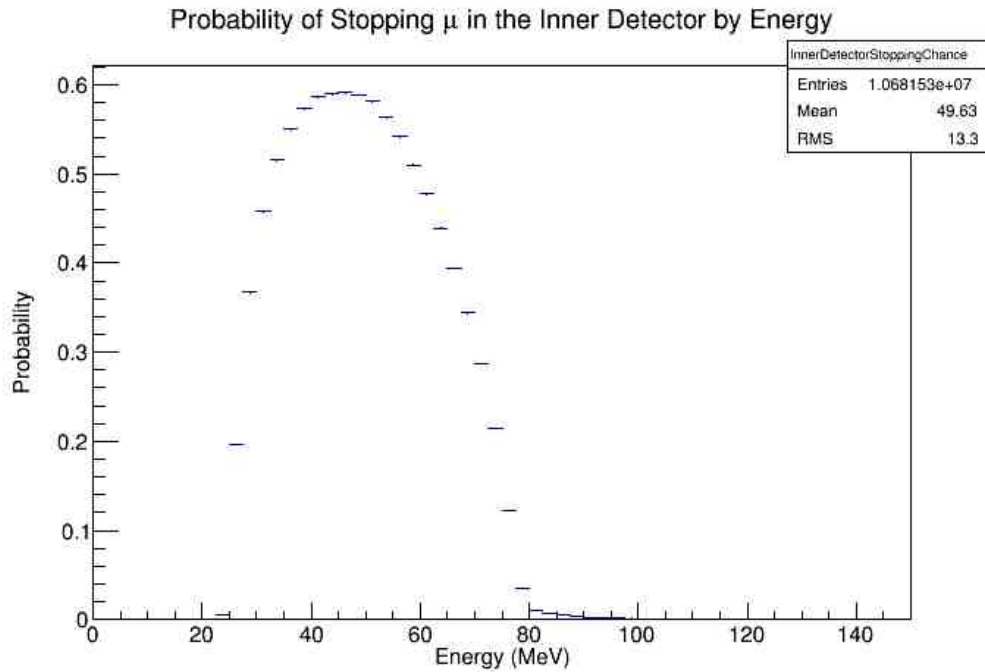


Figure 5.12: Muon stopping probability for the inner detector. The values of this distribution are roughly the same as for just the overall stopping distribution for values above 40 MeV.

analysis of energy spectra was performed to find the likelihood of a muon at a specific energy stopping in the inner detector volume. The results are shown in Fig. 5.12. The results for muons above 40 MeV in energy are similar in value to the overall stopping probability. The overall stopping probability also accounts for muons that stop in the scintillating veto itself, so forms a better overall picture of where all Stopped Muon Monitor signal comes from.

5.4 Beamline Ramifications

The ability to use a stopping weighting function in the beamline Monte Carlo allows for new analyses that provide specific information about actual muon monitor response under beam conditions. The first analysis performed was similar to the tests done to determine overall angular acceptance. A set of 10,000 random detector centers were chosen in the second tracking plane (the one behind the first set of steel shielding) and all direct muon hits in this area were recorded. Each muon's energy was also taken and the overall muon hit was weighted by the probability of the muon stopping. Also recorded was the distance from the origin which corresponds to the distance from the center of the beam spot. A data set comprising the number of stopped muons seen, and the distance from the center of the beamline was created. From there, a profile of the data was taken which plots the average number of stopping muons seen at a given distance from the center of the beamline. The results of this can be seen in Fig. 5.13. This analysis was repeated again at the third and fourth tracking planes (behind the second and third layers of steel shielding respectively) and similar data sets were created. The combined results are shown in Fig. 5.14. This set of data is significant since it represents actual response under a beam pulse.

Using this data it is also possible to make generalizations about how the detector will need to be gated and timed so that it will not be over-saturated. Using the standard radioactive decay formula:

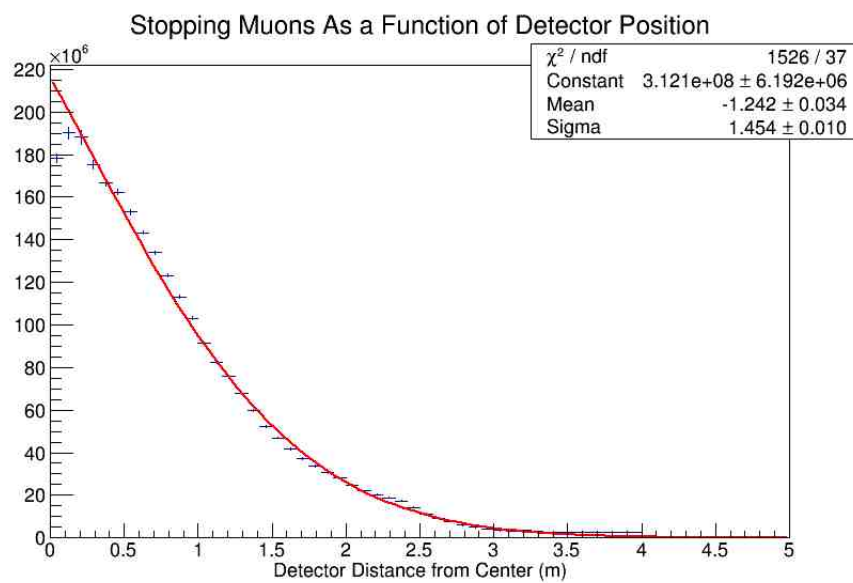


Figure 5.13: Number of stopping muons seen in a detector after the first shielding block. The red fit function was ultimately not used, but the data-points themselves are still relevant. This set of data has been normalized to a regular beam pulse, which is 10^{14} POT

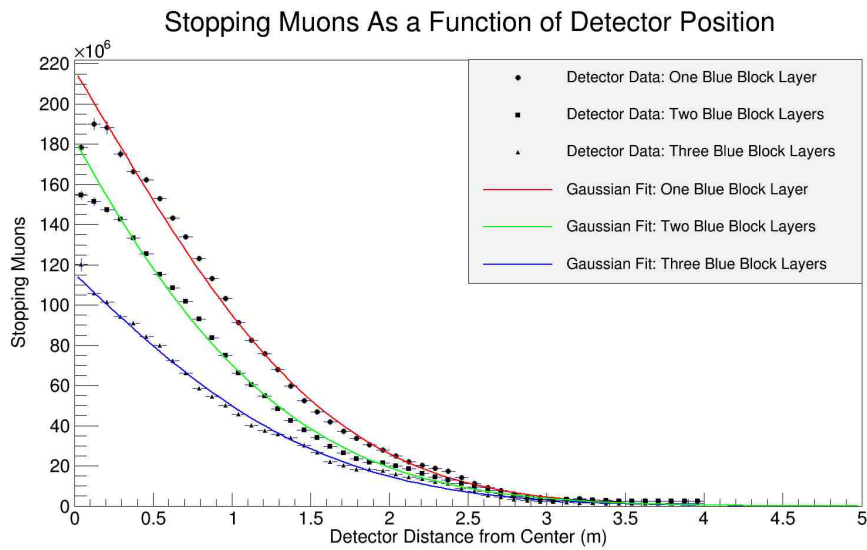


Figure 5.14: Stopping muons seen in detectors as a function of shielding and distance from the beamline. This represents all stopping muons seen in the beam pulse. The gaussian fits to the data ultimately went unused, but the data itself is still useful. This data is normalized to a beam pulse, representing 10^{14} POT. It is worth noting from this figure that we see clear drop off between shielding layers as we would expect, and as detectors move progressively further away from the center of the beam.

$$N(t) = N_0 e^{-t/\tau}, \quad (5.3)$$

where $N(t)$ is the population at time t , N_0 is the initial population, and τ is the average lifetime of a particle (for a muon this is about $2.196 \mu\text{s}$, with variations between μ^+ and μ^- for capture chance on a material). If one applies this to each individual bin in Fig. 5.14, we can calculate how long one would expect it to take until a certain number of muons are seen in the detector. It is estimated for the Stopped Muon Monitor this number is probably ≈ 50 muons (with individual variations up to order of magnitude). 50 muons is chosen as a best guess estimate for good detector resolution between events. The radioactive decay formula was applied bin by bin to the data for stopped muons in a beam pulse, the results of which are in Fig. 5.15. Being able to predict the amount of time needed until reasonable signal is seen allows the electronics to be calibrated to observe the signal at an optimal time. This avoids saturating the PMTs or missing the muons entirely.

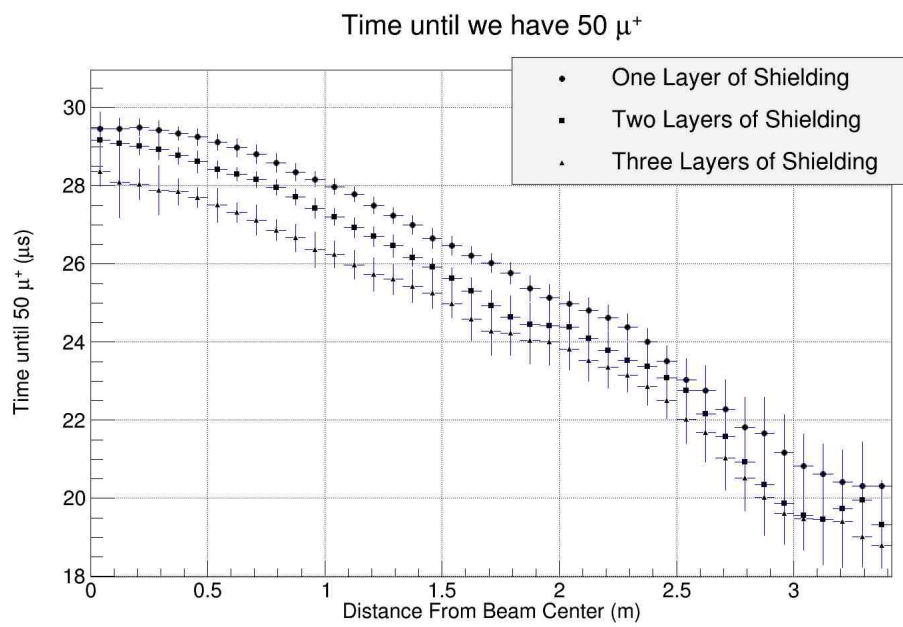


Figure 5.15: Estimation of timing until the Stopped Muon Monitor sees reasonable muon signal (≈ 50 muons).

5.5 Simulations Under Different Physics

As a part of Geant4’s modularity, varying physics models can be assembled into the “physics lists” that handle the physical processes in a simulation run. Changing physics lists can be used as an artificial reweighting of all particle results that come from the beamline Monte Carlo. The default G4LBNE physics list is called “QGSP_BERT”. The details of this physics model is not handled here as it is outside the scope of this thesis. There is a secondary model of physics that can be used in the beamline Monte Carlo called “FTFP_BERT” physics[13]. By comparing between QGSP and FTFP physics, results can be obtained for both the muon monitors and near and far neutrino detectors. With that data, it should be possible to create a mathematical model relating stopping muon signal seen through the absorber hall, to the neutrino flux seen at the near and far neutrino detector. This will help to further constrain the expected neutrino flux seen at both detectors.

To start studying this relation, data sets for the FTFP physics were collected. With FTFP physics enabled, another set of 10^7 POT were simulated in the beamline Monte Carlo. The resulting data was of the same format that the previous QGSP data was, so a similar analysis was applied. Randomized detector positions were selected all through the tracking planes, and using the stopping weight function, total stopping signal was calculated. We can compare this total stopping signal seen under FTFP physics to the original set to start studying differences. The result is seen in Fig. 5.16.

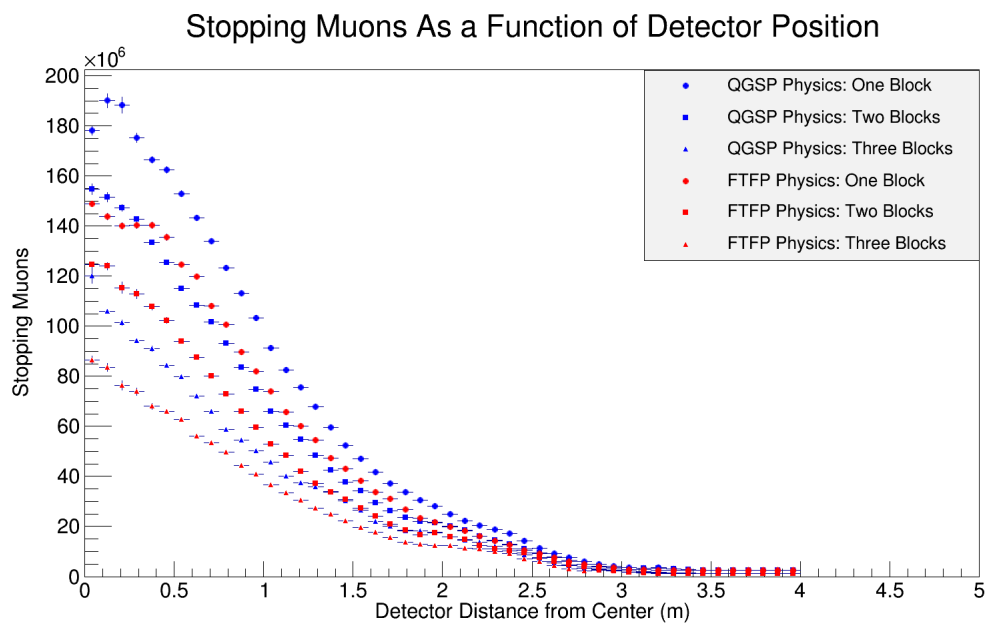


Figure 5.16: Stopping muon signal for FTFP and QGSP physics. The “Blocks” in the legend refer to the steel shielding blocks. On the whole FTFP physics seems to see far fewer muons.

Chapter 6

Future Work and Conclusions

6.1 Future Work

To continue studying how muon monitor measurements can be used to constrain near and far detector neutrino measurements, more simulation and analysis of the beamline Monte Carlo using FTFP physics are needed. Detailed calculation of the near and far neutrino detector flux is required for the FTFP physics so it can be compared to the QGSP derived neutrino flux. Once neutrino flux as a function of energy is understood, differences between FTFP to QGSP fluxes vs energy can be constructed. The process for studying the difference between FTFP stopping muons and QGSP stopping muons has already been started, but more analogous comparisons of relevant kinematic parameters are needed. Once enough of the measurable parameters are understood for both FTFP and QGSP physics for neutrinos and muons,

covariances between these parameters can be created, and this will serve as a mathematical model for understanding what muon measurements in the Stopped Muon Monitors imply for neutrino fluxes.

6.2 Conclusions

This thesis has reviewed some of the developments of the Stopped Muon Monitor from Monte Carlo studies from the beamline Monte Carlo and the stand alone detector Monte Carlo. The beamline Monte Carlo results about initial post-absorber muon spectra were presented. Using simulated detector faces in the beamline Monte Carlo, information about the angular versus direct acceptance of muons in the Stopped Muon Monitor was presented. Use of the Detector Monte Carlo has resulted in a weighting function that can be applied to large data sets from the beamline Monte Carlo to determine which muons form the stopping muon signal seen in the detector itself. Some results of this were presented, including plots of how much signal could be expected at specific distances away from the beam center for a given amount of shielding, in essence allowing reconstruction of a beam pulse for an arbitrary detector layout. This also allows for accurate predictions of the timing necessary in the electronics to ensure that the right amount of signal is seen. Some initial results from the use of different physics runs on the beamline Monte Carlo were presented. Future work should center around using this different physics list methodology to relate differences in neutrino flux to dif-

ferences in muon parameters to create a mathematical model for muons that constrains the overall neutrino flux.

Bibliography

- [1] Giunti, C., (2007) *Neutrino flavour states and the quantum theory of neutrino oscillations*. Journal of Physics G-Nuclear and Particle Physics
- [2] Bishai, M., et al. (2015) *DUNE/LBNF CDR Volume 2: The Physics Program for DUNE at LBNF*. Online at <http://docs.dunescience.org/>
- [3] LBNE Collaboration. (2014) *The Long-Baseline Neutrino Experiment: Exploring Fundamental Symmetries of the Universe*.
Online at the arXiv # 1307.7335
- [4] Beringer, J., et al. (Particle Data Group) (2012) *Particle Physics Booklet*. Extracted from the *Review of Particle Physics* J. Beringer et al. (Particle Data Group) Phys. Rev. D **86** 010001 (2012)
- [5] Bishai, M., et al. (2015) *DUNE/LBNF CDR Volume 1: The LBNF and DUNE Projects*. Online at <http://docs.dunescience.org/>

- [6] Hamernik, T., et al. (2015) *LBNF/DUNE CDR Volume 3: The Long-Baseline Neutrino Facility for DUNE*. Online at <http://docs.dunescience.org/>
- [7] Goodman, M., et al. (2015) *DUNE/LBNF CDR Volume 4: The DUNE Detectors at LBNF*. Online at <http://docs.dunescience.org/>
- [8] Raaf, J. L., et al. (2002) *Mineral oil tests for the MiniBooNE detector* IEEE Transactions on Nuclear Science
- [9] Bolotovskii, B. M. (2009) *Vavilov Cherenkov radiation: its discovery and application* Physics-Uspekhi
- [10] Agostinelli, S., et al. (2003) *Geant4 - A Simulation Toolkit*. Nuclear Instruments and Methods **A** 250-303
- [11] Rene Brun and Fons Rademakers, (1997) *ROOT - An Object Oriented Data Analysis Framework*. Proceedings AIHENP'96 Workshop, Lausanne, Sep. 1996, Nucl. Inst. & Meth. in Phys. Res. A 389 81-86. See also <http://root.cern.ch/>
- [12] Weisstein, Eric W. "Gompertz Curve." From MathWorld—A Wolfram Web Resource. <http://mathworld.wolfram.com/GompertzCurve.html>
- [13] Geant4 Collaboration, Reference Physics Lists. Retrieved March 24, 2016, from http://geant4.cern.ch/support/proc_mod_catalog/physics_lists/referencePL.shtml